JPn Neuroscience
The Journal of Physiology

Electrical synapses and the development of inhibitory circuits in the thalamus

Timothy A. Zolnik[1,2] and Barry W. Connors[1]

[1] *Department of Neuroscience, Division of Biology & Medicine, Brown University, Providence, RI, USA*
[2] *Charité Universitätsmedizin Berlin, Berlin, Germany*

Key points

- The thalamus is a structure critical for information processing and transfer to the cortex.
- Thalamic reticular neurons are inhibitory cells interconnected by electrical synapses, most of which require the gap junction protein connexin36 (Cx36).
- We investigated whether electrical synapses play a role in the maturation of thalamic networks by studying neurons in mice with and without Cx36.
- When Cx36 was deleted, inhibitory synapses were more numerous, although both divergent inhibitory connectivity and dendritic complexity were reduced. Surprisingly, we observed non-Cx36-dependent electrical synapses with unusual biophysical properties interconnecting some reticular neurons in mice lacking Cx36.
- The results of the present study suggest an important role for Cx36-dependent electrical synapses in the development of thalamic circuits.

Abstract Neurons within the mature thalamic reticular nucleus (TRN) powerfully inhibit ventrobasal (VB) thalamic relay neurons via GABAergic synapses. TRN neurons are also coupled to one another by electrical synapses that depend strongly on the gap junction protein connexin36 (Cx36). Electrical synapses in the TRN precede the postnatal development of TRN-to-VB inhibition. We investigated how the deletion of Cx36 affects the maturation of TRN and VB neurons, electrical coupling and GABAergic synapses by studying wild-type (WT) and Cx36 knockout (KO) mice. The incidence and strength of electrical coupling in TRN was sharply reduced, but not abolished, in KO mice. Surprisingly, electrical synapses between Cx36-KO neurons had faster voltage-dependent decay kinetics and conductance asymmetry (rectification) than did electrical synapses between WT neurons. The properties of TRN-mediated inhibition in VB also depended on the Cx36 genotype. Deletion of Cx36 increased the frequency and shifted the amplitude distributions of miniature IPSCs, whereas the paired-pulse ratio of evoked IPSCs was unaffected, suggesting that the absence of Cx36 led to an increase in GABAergic synaptic contacts. VB neurons from Cx36-KO mice also tended to have simpler dendritic trees and fewer divergent inputs from the TRN compared to WT cells. The findings obtained in the present study suggest that proper development of thalamic inhibitory circuitry, neuronal morphology, TRN cell function and electrical coupling requires Cx36. In the absence of Cx36, some TRN neurons express asymmetric electrical coupling mediated by other unidentified connexin subtypes.

(Received 18 November 2015; accepted after revision 5 February 2016; first published online 10 February 2016)
Corresponding author T. A. Zolnik: Charité Universitätsmedizin Berlin, 10117 Berlin, Germany.
Email: timothy_zolnik@alumni.brown.edu

Abbreviations aCSF, artificial cerebrospinal fluid; CCf, coupling coefficient; C_{in}, input capacitance; cIPSC, coincident IPSC; Cx36, connexin36; G_j, junctional conductance; KO, knockout; mIPSC, miniature IPSC; R_{in}, input resistance; TRN, thalamic reticular nucleus; VB, ventrobasal nucleus; V_j, junctional voltage; WT, wild-type.

DOI: 10.1113/JP271880

Introduction

Neuronal gap junctions (electrical synapses) mediate rapid, bidirectional communication. Electrical synapses may have diverse functions, including synchronizing activity (Bennett and Zukin, 2004), mediating intercellular molecular signalling (Harris, 2001) and contributing to cell adhesion (Elias *et al.* 2007). A long-standing yet poorly understood issue is the role of electrical synapses during neural circuit development (Fischbach, 1972; Connors *et al.* 1983; Kandler and Katz, 1995, 1998*a*, 1998*b*; Roerig and Feller, 2000; Montoro and Yuste, 2004; Sutor and Hagerty, 2005; Li *et al.* 2012; Yu *et al.* 2012; Niculescu and Lohmann, 2013). Electrical synapses have been implicated in the proper development of chemical synaptic connections in the mammalian olfactory bulb (Maher *et al.* 2009), retinogeniculate system (Blankenship *et al.* 2011) and neuromuscular junction (Personius *et al.* 2007), as well as other neural systems (Mentis *et al.* 2002; Szabo *et al.* 2004; Arumugam *et al.* 2005; Neunuebel and Zoran, 2005; Szabo and Zoran, 2007; Todd *et al.* 2010). These studies suggest that electrical synapses importantly regulate network development. Most mammalian investigations have focused on glutamatergic synapses (Yu *et al.* 2012; Pereda, 2014), yet the majority of electrically coupled neurons in the forebrain are GABAergic. To test whether electrical synapses are important for inhibitory circuit development, we chose the thalamic reticular nucleus (TRN). The GABAergic TRN neurons are interconnected by electrical synapses (Landisman *et al.* 2002; Long *et al.* 2004) and project their axons onto thalamocortical relay neurons (Pinault, 2004). TRN-mediated inhibition helps to shape receptive field properties of relay neurons (Lee *et al.* 1994) and generate certain types of rhythms associated with sleep and seizure states (Huguenard and McCormick, 2007).

Most mammalian electrical synapses depend on the neuronal gap junction protein connexin36 (Cx36) (Deans *et al.* 2001; Hormuzdi *et al.* 2001; Connors and Long, 2004). TRN neurons are densely interconnected by Cx36-containing gap junction channels (Belluardo *et al.* 2000; Landisman *et al.* 2002; Liu and Jones, 2003), which are present at birth and strengthen over the next 2 weeks (Parker *et al.* 2009). Other connexins may also contribute to neuronal network maturation. Over 20 connexin genes have been identified in the mouse; around half of them are expressed in the brain, mainly in glial cells (Willecke *et al.* 2002; Sohl *et al.* 2005). Only a few connexin subtypes are expressed in central neurons, and only Cx36 has been consistently implicated in electrical coupling in the mammalian brain (Connors & Long, 2004; Pereda, 2014). Each connexin subtype, and in some cases heteromeric or heterotypic combinations of subtypes, can form gap junction channels with distinctive channel properties (Harris, 2001; Rash *et al.* 2013). Cx36, however, does not appear to form heterotypic or heteromeric channels (Koval *et al.* 2014).

Inhibitory synapses undergo extensive remodelling during development (Kim and Kandler, 2003; Hensch and Fagiolini, 2005; Kätzel and Miesenböck, 2014; Froemke, 2015). The thalamic inhibitory circuit changes rapidly and dramatically during the first two postnatal weeks (Warren and Jones, 1997; Lee *et al.* 2010). In the present study, we investigated whether the development of intrathalamic GABAergic synapses and circuits is affected by the deletion of Cx36. The results obtained imply that electrical synapses have a broad influence on the development of thalamic networks.

Methods

Slice preparation

All experiments were approved by the Institutional Animal Care and Use Committee of Brown University. Animals were deeply anaesthetized with propofol prior to preparation of 300 μm-thick thalamocortical slices (Agmon and Connors, 1991) from wild-type (WT) (postnatal ages P0 – P13) and littermate WT and Cx36 knockout (KO) FvB/C57 mice (P2 – P13) of either sex. The experimenter was blind to the genotype during the recording and analyses. Immediately following slice preparation, the slices were incubated at 32°C for 30 min and at room temperature for at least an additional 30 min before recording in a submersion chamber at 32°C. Slices were visualized on an BX50WI microscope (Olympus, Tokyo, Japan) using a CCD camera (Hamamatsu City, Japan) and infrared-differential interference contrast optics.

The artificial cerebrospinal fluid (aCSF) bathing the slices during recording and slicing contained (in mM): 126 NaCl, 3 KCl, 1.25 NaH_2PO_4, 26 $NaHCO_3$, 2 $CaCl_2$, 2 $MgCl_2$ and 10 dextrose, and was saturated with 95% O_2–5% CO_2. In some experiments, 6,7-dinitroqinoxaline-2,3-dione (20 μM) and D-2-amino-5-phosphopentanoic acid (50 μM) were added to the aCSF to block AMPA and NMDA receptors, respectively; to isolate miniature IPSCs (mIPSCs), TTX (1 μM) was added to the aCSF to block sodium channel-dependent spikes.

Recording and imaging

Dual whole-cell current clamp and voltage clamp recordings were made with low resistance (2.5–4 MΩ) microelectrodes. For current clamp recordings, the intracellular solution contained (in mM): 130 K-gluconate, 4 KCl, 2 NaCl, 0.2 EGTA, 10 Hepes, 4 ATP-Mg, 0.3 GTP-Tris and 14 phosphocreatine-Tris. For voltage clamp recordings, the intracellular solution contained (in mM): 54 Cs-gluconate, 56 CsCl, 1 $CaCl_2$, 1 $MgCl_2$, 10 EGTA, 10 Hepes, 5 QX-314, 4 ATP-Mg, 0.3 GTP-Tris

and 14 phosphocreatine-Tris. Both solutions were adjusted to pH 7.25–7.30 (285–295 mosmol). A MultiClamp 700B amplifier (Molecular Devices, Sunnyvale, CA, USA) was used to make simultaneous recordings from pairs of closely apposed (<2 μm) cell somata in the TRN; both cells were held at −60 mV in voltage clamp or at around −60 mV in current clamp by continuous current injection. Single or pairs of relay neurons were also recorded in the ventrobasal (VB) complex. Series resistance was continually monitored and compensated (70–80% in voltage clamp) and was typically between 6 and 20 MΩ before compensation. Recordings were not corrected for liquid junction potential.

Cell capacitance was determined using the built-in capacitance-compensation function of the amplifier. Cell input resistance was determined in current clamp or voltage clamp by measuring the steady-state voltage (in current clamp) or current (in voltage clamp) response from small, 600 ms current (−5 pA to −50 pA for current clamp) or voltage (−10 mV for voltage clamp) steps.

Electrical coupling was measured in voltage clamp by simultaneously stepping both cells to 0 mV and then stepping one or the other cell to −80 mV (Fig. 2*A*) at the same time as recording the holding current in both cells. In current clamp, electrical coupling was measured by injecting hyperpolarizing current into one cell (the driven cell; V_d) to bring it to around −100 mV, at the same time as recording the voltage deflections in the adjacent coupled cell (the follower cell; V_f) and V_d. The coupling coefficient (CCf) is defined as: $CCf = (\Delta V_f/\Delta V_d) \times 100$.

For extracellular stimulation, a tungsten monopolar or concentric biopolar electrode (FHC, Bowdoinham, ME, USA) was placed in the TRN or VB, <200 μm from the recording site. To determine the paired-pulse ratio, two stimuli with a 100 ms interstimulus interval were given at 0.04–0.1 Hz. IPSCs were recorded exclusively in Cs-based internal solution at $V_{hold} = -60$ mV ($E_{Cl} = -20$ mV), filtered at 2 kHz and digitized at 20 kHz.

In some experiments, Alexa Fluor 633 hydrazide dye (75 μM; Invitrogen, Carlsbad, CA, USA) was added to the pipette solution for cell loading and subsequent confocal imaging. Slices with dye-filled neurons were fixed with 4% paraformaldehyde in 0.1 M phosphate buffer for 30 min at room temperature. The slices were then moved to phosphate-buffered saline (< 1 day) until they were mounted on slides with VectaShield (Vector Laboratories, Burlingame, CA, USA) mounting medium. An LSM510 confocal microscope (Carl Zeiss, Oberkochen, Germany) with a 20× Plan-Neofluar (0.8 NA) objective was used for imaging. Images were scanned at 2048 × 2048 pixels. The typical step size per section through the *z*-axis was 1 μm, or occasionally 0.2 μm.

Basic morphological properties of neurons were determined by counting the number of primary dendrites and by measuring the 3-D soma surface area using convex hull analysis in NeuroExplorer (MicroBrightField Inc., Williston, VT, USA) after reconstruction in Auto-Neuron (MicroBrightfield Inc.). Dendritic complexity was quantified using 2-D Sholl analysis (Sholl, 1953) with increments of 10 μm between circles. Total dendritic length was estimated by multiplying the Sholl intersections per circle by the increment distance (10 μm) and taking the sum of all circles. All analysis was performed in ImageJ (NIH, Bethesda, MD, USA), Neuroexplorer and Zeiss LSM Image Browser.

Detection of spontaneous coincident IPSCs

IPSCs were considered coincident between two cells if the onset time of an IPSC in one cell occurred within ±1 ms of the onset time of an IPSC in the other cell. The onset time of an IPSC is the point of downward deflection at the start of the IPSC waveform, and this was measured using optimal fit parameters with Minianalysis (Synaptosoft Inc., Fort Lee, NJ, USA). Spontaneous IPSC onset times were compiled for each neuron pair from 3–5 min of continuously recorded data. Using these data, a custom Matlab (MathWorks Inc., Natick, MA, USA) algorithm was written to test for statistically significant occurrences of cIPSCs. First, the number of coincident IPSCs (cIPSCs) was calculated (see above) by comparing the compiled IPSC onset times from each neuron in a pair and finding paired values within ±1 ms. Second, the inter-IPSC intervals were calculated from the IPSC onset times for each neuron in the pair. Third, the inter-IPSC intervals for each neuron of a pair were measured independently, and randomly shuffled, using a MatLab randomization function, into 10,000 surrogate data sets. Fourth, each surrogate data set was scanned for cIPSCs as was carried out in step one with the real data set. IPSC coincidence was considered significant if 95% of the surrogate data sets had fewer cIPSCs than the real data set.

The expected chance occurrence of cIPSCs was then calculated. The number of IPSCs in each neuron of a pair was determined and divided by the number of milliseconds over which those events occurred to find the probability of an IPSC occurring within a 1 ms bin. This assumes that the IPSCs were independent and randomly distributed across time. The 1 ms bin probability from one neuron was then multiplied by the 1 ms bin probability in the other neuron to obtain the probability of two IPSCs occurring, one in each neuron, within 1 ms. This probability was then multiplied by the duration of the recording to estimate the expected chance occurrences of coincident IPSCs:

Expected chance cIPSCs = (α) x (β) x recording time (ms)

where α = cell A 1 ms bin probability = total IPSCs of cell A/time (ms) and β = cell B 1 ms bin probability = total IPSCs of cell B/time (ms).

Statistical analysis

Gap junctional conductance (G_j) was determined in voltage clamp by:

$$G_j = I_j / V$$

where V_j is the transjunctional voltage and I_j is the resulting junctional current. Cell pairs generally had high input resistance (>150 MΩ) and low coupling conductance (<1 nS) and the series resistance in each electrode was generally less than 6 MΩ after compensation. Therefore, minimal error in G_j is expected from these factors (Van Rijen *et al.* 1998). In current clamp, G_j was calculated as (Bennett, 1966):

$$G_j = 1 / \frac{[R_{in(1)} * R_{in(2)} - R_{tr}{}^2]}{R_{tr}}$$

where $R_{in(x)}$ is the input resistance of each cell in a recorded pair and R_{tr} (transfer resistance) is the value of the voltage response in the follower cell divided by the current amplitude injected into the driven cell.

The decay time constant of the junctional conductance was determined by fitting a single exponential (Fig. 2).

The frequency of mIPSCs was determined by counting events from raw data traces using pClamp, version 10.2 (Molecular Devices). mIPSCs were also identified by template matching in pClamp. More than 50 mIPSCs were averaged to determine the mean mIPSC amplitude and decay time for each cell. mIPSC amplitude was defined as the difference between the mean holding current in a 10 ms window before the onset of the mIPSC and the mean current during a 1–2 ms window centered on the peak of the mIPSC. Falling phases of the mIPSCs were fit with a double exponential ($I = A_1 \exp -^{t/}\tau_{D1} + A_2 e -^{t/}\tau_{D2}$), which was used to determine the weighted decay time constant from $\tau_{IPSC} = (\tau_{D1}A_1 + \tau_{D2}A_2)/(A_1 + A_2)$ (Huntsman and Huguenard, 2000).

$P < 0.05$ was considered statistically significant. Data are reported as the mean ± SE. Multiple linear regression analysis and Student's t test were used to compare genotype and age differences. The Kolomogorov–Smirnov two sample test was used to compare genotype differences in amplitude distribution histograms.

Results

Electrical synapses in the TRN

In many brain areas, the prevalence of electrical coupling is greatest during early development and declines with age. In the TRN, however, electrical synapses are ubiquitous as early as the day of birth (Parker *et al.* 2009), and coupling conductance steadily strengthens by P14–18. In the mature mouse, electrical coupling is largely dependent on Cx36 (Landisman *et al.* 2002). Consistent with these results, we found that the probability of electrical coupling between neuron pairs was stable across the first 2 weeks of development in the WT TRN (mean of 68.6% coupling probability, $n = 105$ pairs) and, in neurons from Cx36 KO mice, the coupling probability was more than five-fold less (mean of 12.4% coupling probability, $n = 129$ pairs) (Fig. 1*A* and *B*). The prevalence of electrical coupling in the KO TRN was not influenced by age. This suggests that the large majority of electrical coupling in TRN requires Cx36

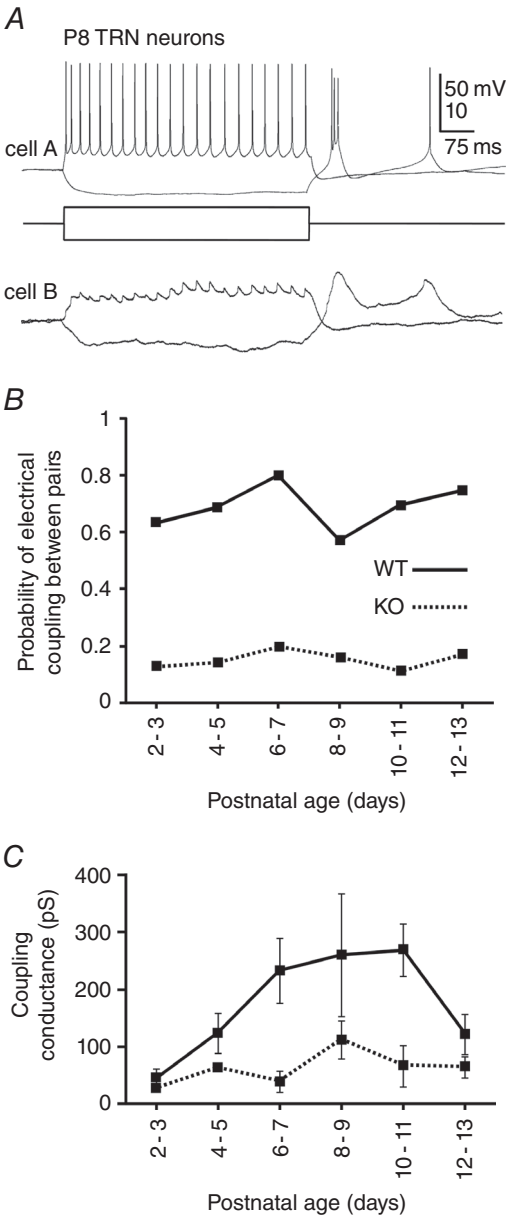

Figure 1. Electrical coupling in the TRN
A, current clamp recording of electrical coupling between two TRN neurons aged P8. The incidence (*B*) and mean ± SEM conductance (*C*) of electrical coupling between adjacent neuron pairs during development. Data in (*B*) and (*C*) are taken from 105 WT and 129 KO pairs.

at all ages tested but that non-Cx36-dependent electrical synapses can also form between TRN cells. These results are consistent with a study from our laboratory reporting significant dye-coupling among TRN neurons from Cx36 KO mice (Lee *et al.* 2014).

Among the measurable electrical synapses that we observed, the mean coupling conductance (G_j) between KO cell pairs was less than one-third that of WT pairs (WT, 190.3 pS, $n = 64$; KO, 60.9 pS, $n = 16$) (Fig. 1*C*). Thus, electrical synapses were both dramatically sparser and weaker in the absence of Cx36. Coupling between WT cells showed a significant age-dependent increase in G_j, whereas G_j in the KO did not have an age-dependent change (WT, $P = 0.05$; KO, $P = 0.38$, linear regression) (Fig. 1*C*). The conductance decrease that we measured between P10–11 to P12–13 was not significant ($P = 0.27$, post-hoc Tukey's honestly significant difference test) and thus may not indicate a deviation from previous results (Parker *et al.* 2009). Despite a much lower G_j in the KO cells overall, the CCf (see Methods) were, on average, only modestly lower than in WT cells (WT, CCf = 6.8%, $n = 72$; KO, CCf = 4.8%, $n = 16$).

The product (CCf × $P_{coupling}$) provides an overall measure of electrical coupling within the TRN network (Amitai *et al.* 2002). Collapsed across development, this measure is 4.7 for the WT and 0.6 for the KO samples, suggesting that deletion of Cx36 reduces the influence of electrical synapses by more than 85% during the first two postnatal weeks. Overall, our data suggest that electrical coupling in the TRN of WT cells remains stable and largely but not entirely dependent upon Cx36 during postnatal development.

Properties of non-Cx36-dependent electrical synapses

As described above, some electrical coupling remains between TRN neurons of the Cx36-KO. The properties of non-Cx36 gap junctions have not been described previously in central mammalian neurons, and so these were examined further. All vertebrate gap junctions have some voltage-dependence; in every case, G_j is maximal when transjunctional voltage (V_j) is zero, and G_j declines as V_j deviates from zero. Both the steepness of the voltage-dependence of G_j and the time constant (τ) of its decline vary widely but characteristically with connexin subtype (Moreno *et al.* 1995; Teubner *et al.* 2000; Bukauskas *et al.* 2006). The G_j for Cx36 gap junctions is almost insensitive to V_j over the range of ±50 mV (Teubner *et al.* 2000). Other gap junction channels, including those comprised of Cx45, have a considerably steeper voltage-dependence (Moreno *et al.* 1995). Because Cx45 is one of the few connexins besides Cx36 that is expressed in thalamic neurons (Willecke *et al.* 2002; Sohl *et al.* 2005), it is a prime candidate for mediating electrical coupling in the Cx36 KO.

We performed dual voltage clamp measurements in pairs of TRN neurons to measure the gating properties of their electrical synapses (Fig. 2*A*). Consistent with previous work on Cx36 junctions (Teubner *et al.* 2000), we found that its gating was slow. In pairs of coupled neurons from the Cx36 KO, however, the τ of G_j decline was much faster compared to WT junctions. During a 600 ms, 80 mV transjunctional step, the τ of G_j decline was 490 ms for WT and 151 ms for KO connections (Fig. 2*B*). Some invertebrate electrical synapses have distinctly asymmetric conductances when measured in each direction across the junction (Furshpan and Potter, 1959; Jaslove and Brink, 1986). The large majority of electrical synapses among vertebrate central neurons are symmetric (Connors and Long, 2004), although a few exceptions have been described (Auerbach and Bennett, 1969; Haas *et al.* 2011; Rash *et al.* 2013; Sevetson and Haas, 2015). Gap junction asymmetry may arise from heterotypic hemichannels (Phelan *et al.* 2008). We found that electrical synapses from Cx36-KO neurons, but not from WT cells, often had asymmetric G_j. Examples of symmetric WT and asymmetric KO junctions are shown in Fig. 3*A*. In each coupled cell pair, G_j was measured in each direction and a G_j ratio was defined as G_j(weaker)/G_j(stronger). The G_j ratio was significantly lower in junctions from KO than from WT cells (WT, mean G_j ratio 0.85, $n = 35$; KO, mean G_j ratio 0.53, $n = 12$; $P = 0.006$) (Fig. 3*B*). One possible source of error in estimating G_j asymmetry could be differences in the R_{in} of coupled cell pairs in the KO. However, the R_{in} ratio was not significantly different between WT and KO cell pairs ($P = 0.81$) and the G_j ratios were not correlated with the R_{in} ratios (Fig. 3*B*). The enhanced G_j asymmetry of KO junctions suggests that asymmetry might be related to the relative weakness of KO electrical synapses. We plotted the average junctional current for each cell in a pair against the G_j ratio for that pair; even weak WT synapses with low

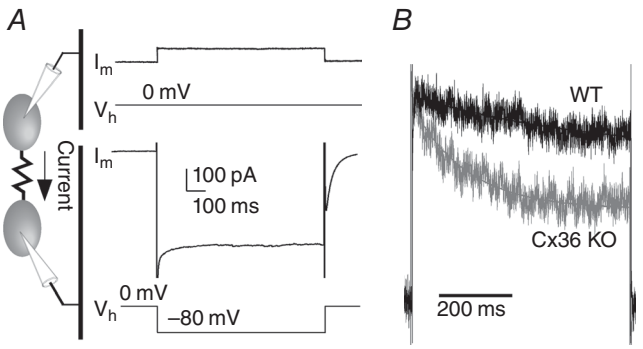

Figure 2. Effect of Cx36 genotype on voltage-dependent kinetics of electrical coupling in the TRN
A, protocol for measuring electrical coupling in voltage clamp (see Methods). *B*, overlay of the junctional current from WT (black) and Cx36 KO (grey) neuron pairs. Current amplitudes are normalized.

junctional currents passed current quite symmetrically, whereas KO synapses tended to be much more asymmetric (Fig. 3*C*). We conclude that non-Cx36 electrical synapses in TRN are often asymmetric (i.e. rectifying).

Morphology and intrinsic physiology of TRN neurons

We next tested whether the absence of Cx36 in the TRN network affected the morphology and intrinsic physiology of TRN neurons. We first quantified dendritic arbors and soma surface area during early (P2–5) and later (P10–13) periods in postnatal development (Fig. 4*A*) (see Methods). The complexity of dendritic arbors in TRN neurons increased during development, as indicated by an age-dependent rise in the number of Sholl intersections (Fig. 4*B*) and a larger total dendritic length (Fig. 4*C*). Cx36 genotype did not significantly affect the number of primary dendrites or dendritic length (Fig. 4*C*). The dendritic complexity assessed by Sholl intersection frequency was also unaffected (P2–5, $P = 0.97$; P10–13, $P = 0.79$; Kolmogorov–Smirnov test) (Fig. 4*B*). At P2–5, the mean surface area of TRN somata was larger in KO cells ($1961 \pm 267\ \mu m^2$) than in WT cells ($1076 \pm 153\ \mu m^2$, $P = 0.014$), although somata did not differ significantly at older ages (P10–13, KO *vs.* WT, $P = 0.97$) (Fig. 4*C*).

Electrical coupling among neurons can also affect their intrinsic physiological properties; in neocortical interneurons, for example, coupling accounts for around half of each cell's input conductance (the inverse of input conductance is input resistance, R_{in}; Amitai *et al.* 2002). Consistent with this, we found that R_{in} was significantly higher in KO cells than in WT cells ($P < 0.001$, $r = 0.74$, multiple linear regression) (Fig. 5*A*). Between P2 and P13, the R_{in} of TRN neurons decreased by more than five-fold in both genotypes. Input capacitance, C_{in}, a measure of cell surface area, increased considerably with age, which is consistent with the results of previous studies (Parker *et al.* 2009; Lee *et al.* 2010), although there was no significant difference between Cx36 genotypes ($P = 0.31$, $r = 0.57$) (Fig. 5*B*). Overall, these results indicate that the input resistance is affected by the Cx36 genotype in TRN neurons and dendritic size and complexity increases dramatically with age.

Inhibitory synaptic currents in VB relay neurons

Synaptic properties change dramatically during network development, and gap junctional coupling has often been implicated in this process (Roerig and Feller, 2000). We tested whether the synaptic inputs to VB neurons from TRN were affected by the deletion of Cx36. We first recorded $GABA_A$-dependent (Fig. 6*A*) mIPSCs in VB cells in the presence of glutamate receptor antagonists and TTX. The mIPSC frequency increased dramatically across age until P8–9, after which it stabilized (Fig. 6*B*). Cx36 genotype also affected mIPSC frequency; mIPSC frequencies were significantly higher in KO cells than in WT cells ($P = 0.004$, Kolmogorov–Smirnov test) (Fig. 6*B*). The difference between genotypes appeared at around P4–5, although the time-course of the age-dependent increase in mIPSC frequency was unaffected by genotype.

The decay time constants of mIPSCs (τ_{IPSC}) became progressively faster between P0–1 and P12–13 in VB (Fig. 6*B* and *C*), decreasing by ~62% during this period. Cx36 genotype did not have a significant effect on τ_{IPSC}. The mIPSC amplitudes also changed with age, falling slightly after P6–9 (Fig. 6*B*). Cx36 genotype influenced the distributions of mIPSC amplitudes (Fig. 6*D*). At both

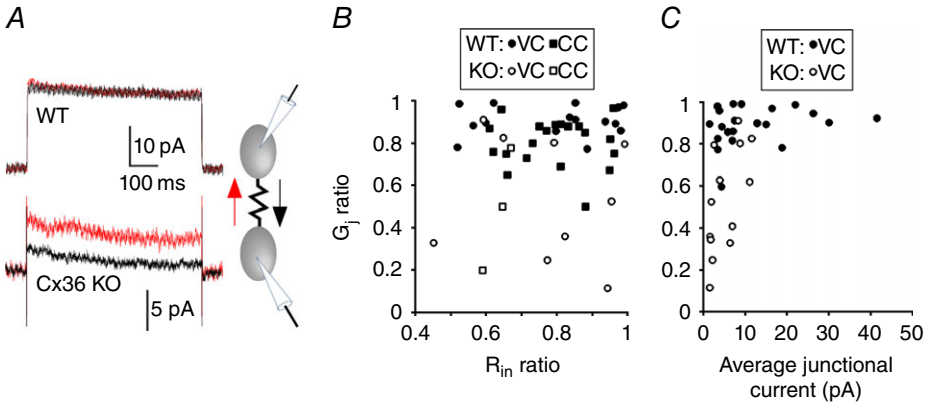

Figure 3. Effect of Cx36 genotype on the asymmetry of electrical coupling in TRN
A, junctional currents induced by +80 mV and –80 mV transjunctional voltage steps (black and red traces, respectively). Junctional currents in the WT pair are similar in both directions. Junctional currents in the KO pair are direction-dependent (i.e. asymmetric). *B*, relationship between junctional coupling asymmetry (G_j ratio) and input resistance (R_{in} ratio) among WT and KO neuron pairs. *C*, coupling asymmetry *vs.* mean coupling strength (pA) between WT and KO neuron pairs. Each symbol in (*B*) and (*C*) represents data from a neuron pair of the type as specified in the insets (VC, voltage clamp; CC, current clamp measurements).

P2–5 and P12–13, the difference in amplitude distribution was significantly shifted to larger amplitudes in the Cx36 KO (P2–5: $P = 0.00001$, $n = 1743$, $n = 12$ cells for each genotype; P12–13: $P < 0.00001$, $n = 1869$, $n = 4$ cells for each genotype; Kolmogorov–Smirnov test). These data suggest that the absence of Cx36 leads to a distribution of larger mIPSC amplitudes in VB neurons.

Evoked IPSCs were triggered with paired (100 ms interval) extracellular stimuli to test the effects of Cx36 deletion on presynaptic mechanisms. In WT-VB neurons, the second IPSC was depressed relative to the first (paired-pulse ratios = 0.55) (Fig. 6*E*). Cx36 genotype did not have a significant effect on the paired-pulse ratio ($P = 0.96$).

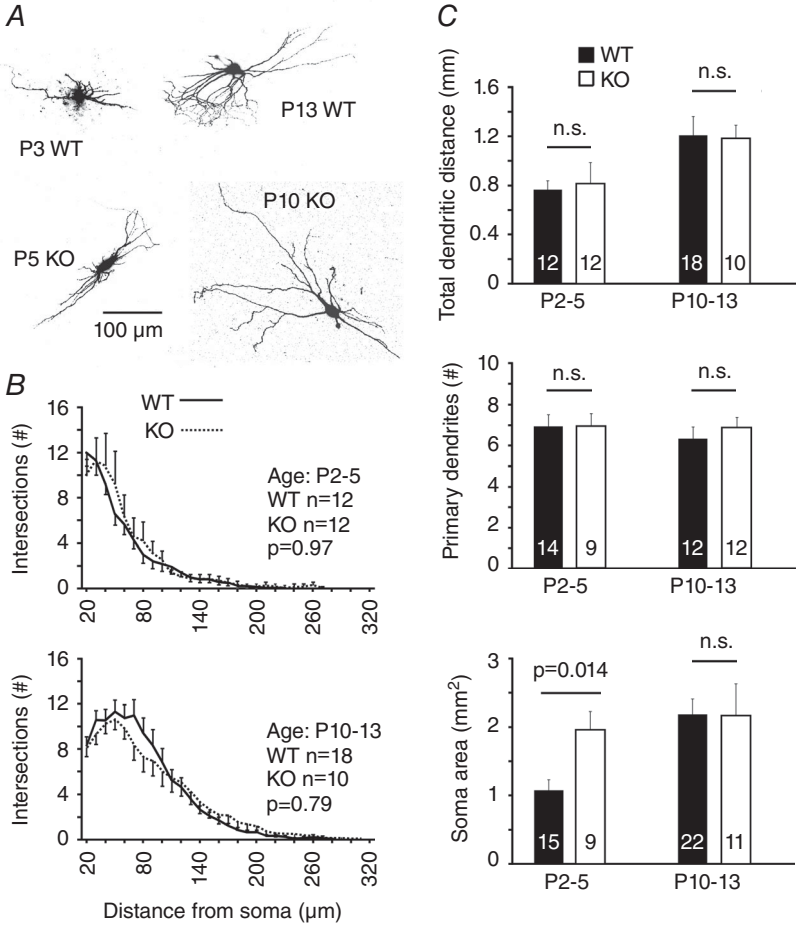

Figure 4. Morphology of TRN neurons by Cx36 genotype and age
A, photomicrographs of example neurons used for morphological analysis. *B*, counts of Sholl intersections by distance from the soma (mean ± SEM) by genotype and age group. *P* values are from a Kolmogorov–Smirnov test. *C*, morphological characteristics determined from Sholl intersections and 3-D reconstruction of somata. Numbers of sampled neurons for each group are indicated on the bars. n.s., not significant.

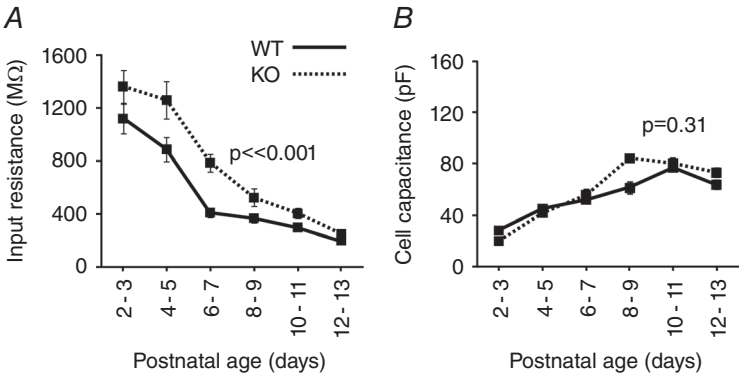

Figure 5. Passive membrane properties of TRN neurons as a function of age and Cx36 genotype
A, input resistance declined with age and was significantly higher in KO neurons ($P < 0.001$, $r = 0.74$). *B*, cell capacitance increased with age and was unaffected by genotype ($P = 0.31$, $r = 0.57$). *P* values were determined based on linear regression. A total of 305 neurons was sampled (159 WT and 146 KO neurons); *n* for each genotype per 2 day age group ranged from 12 to 39 neurons.

When recording spontaneous IPSCs simultaneously from pairs of neighbouring VB neurons (without TTX), we found that some IPSCs occurred coincidently, with onsets within ±1 ms of each other, suggesting that they may have been driven by a common presynaptic TRN neuron (Fig. 7*A*). By comparing the frequency of cIPSCs in recordings to sets of randomly shuffled IPSC timings (see Methods), we found that some neuron pairs appeared to have cIPSCs above chance levels, consistent with common presynaptic inputs. At younger ages, P5–P9, almost half of WT and KO cell pairs had cIPSCs, and there was no significant difference by genotype ($P = 0.34$, Fisher's exact test) (Fig. 7*B*). Interestingly, whereas older WT cell pairs (P10–P13) also generated cIPSCs, none of the tested KO pairs had cIPSCs ($P = 0.02$, Fisher's exact test) (Fig. 7*B*). This result suggests that the absence of Cx36 leads to less divergence of TRN inputs onto VB neurons.

Taken together, greater mIPSC frequency and a lack of paired-pulse effects implies more GABAergic release sites, and fewer cIPSCs suggests a decrease in divergent inputs on KO-VB neurons.

Morphology and intrinsic physiology of VB neurons

We next tested whether the morphology and intrinsic physiological properties of VB neurons were affected by the deletion of Cx36. VB neurons were filled intracellularly with Alexa dye at ages P2–5 or P10–13

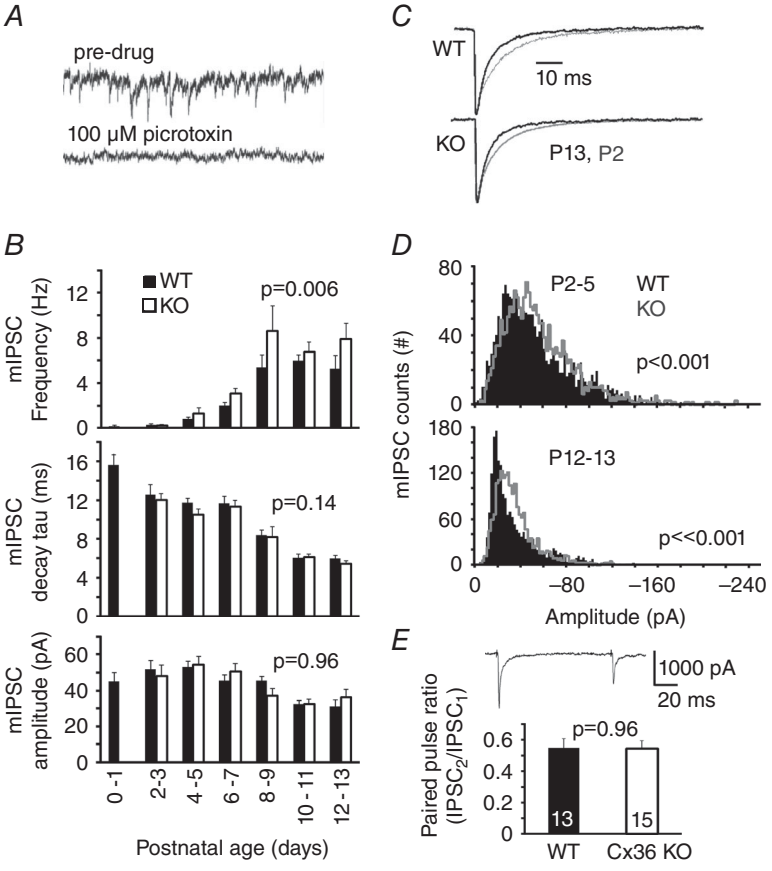

Figure 6. Effects of Cx36 genotype on the properties of IPSCs in VB relay neurons
A, examples of mIPSCs and sensitivity to picrotoxin, a $GABA_A$ receptor antagonist. *B*, mIPSC properties as a function of age and Cx36 genotype. mIPSC frequency is significantly higher in the KO compared to WT ($P = 0.006$, $r = 0.53$) ($n = 175$ neurons; 84 KO, 91 WT). The mIPSC decay rate (τ_{IPSC}, $P = 0.14$, $r = 0.72$) and amplitude ($P = 0.96$, $r = 0.46$) were not affected by genotype. Bars plot the mean ± SEM for each age and genotype group; *P* values are based on linear regression. *C*, examples of WT and KO mIPSCs compared at P2 and P13. Each trace is the average of 40 mIPSCs, with amplitudes normalized. *D*, mIPSC amplitude frequency histogram for P2–5 ($n = 12$ neurons for each genotype) and P12–13 ($n = 4$ neurons for each genotype). *P* values from the Kolmogorov–Smirnov test. *E*, paired-pulse ratio of evoked IPSCs. Bar graph shows the mean ± SEM, with sample numbers specified on each bar. Inset: example trace of IPSCs from a WT cell.

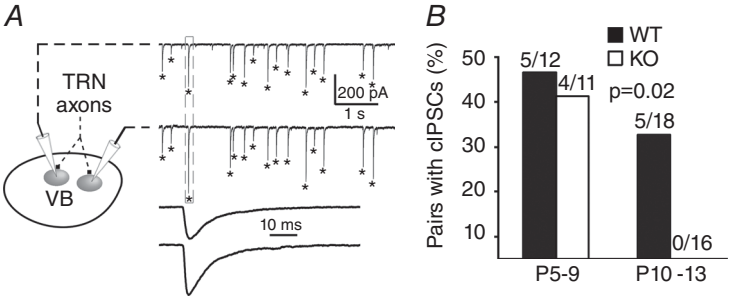

Figure 7. Coincident IPSCs from VB neuron pairs
A, example of cIPSCs; asterisks indicate IPSCs that are coincident (i.e. peaks within ±1 ms of each other). The box indicates the cIPSCs shown at a fast time scale below. *B*, prevalence of neuron pairs with statistically significant occurrences of cIPSCs by age range (see Methods).

(Fig. 8*A*). Interestingly, the frequency of Sholl intersections, and thus dendritic complexity, was significantly lower in KO neurons than WT neurons in the P10–13 age groups between 20 and 200 μm from the soma ($P = 0.03$, Kolmogorov–Smirnov) (Fig. 8*B*), the region of greatest dendritic branching and complexity in these neurons. There was, however, no difference in intersection frequency in the younger P2–P5 age group by genotype between 20 and 140 μm from the soma ($P = 0.81$, Kolmogorov–Smirnov) (Fig. 8*B*). The total dendritic distance measured from Sholl intersection frequency data tended to be larger in the WT than the KO but did not reach significance ($P = 0.07$) (Fig. 8*B*). The number of primary dendrites was unaffected by genotype or age (Fig. 8*C*). The 3-D surface areas of VB somata were not significantly different by genotype (Fig. 8*C*).

As with TRN neurons, the R_{in} of neurons in VB sharply decreased with age (Fig. 9*A*), falling by more than three-fold; in contrast to TRN neurons, the R_{in} of VB neurons did not differ significantly by genotype ($P = 0.66$, $r = 0.73$, multiple linear regression). C_{in} increased considerably with age in VB cells but did not differ between Cx36 genotypes ($P = 0.17$, $r = 0.61$) (Fig. 9*B*).

Our results indicate that the Cx36 KO genotype leads to less complex dendritic arbors of VB neurons while maintaining the same number of primary dendrites and soma size. R_{in} decreases with age and C_{in} increases with age, although they do not depend on the Cx36 genotype.

Discussion

The results of the present study demonstrate that the deletion of Cx36 leads to alterations in electrical coupling, neuron morphology, intrinsic physiology and inhibitory synapse functions during the early postnatal maturation of thalamic networks. This implies that electrical synapses play a significant role in the formation of inhibitory thalamic circuits.

Cx36 and electrical synapse asymmetry

The incidence of electrical coupling in the WT-TRN remained high and steady during the first two postnatal weeks, and junctional conductance increased during this period (Fig. 1), consistent with a previous study (Parker *et al.* 2009). Some electrical connections remained between

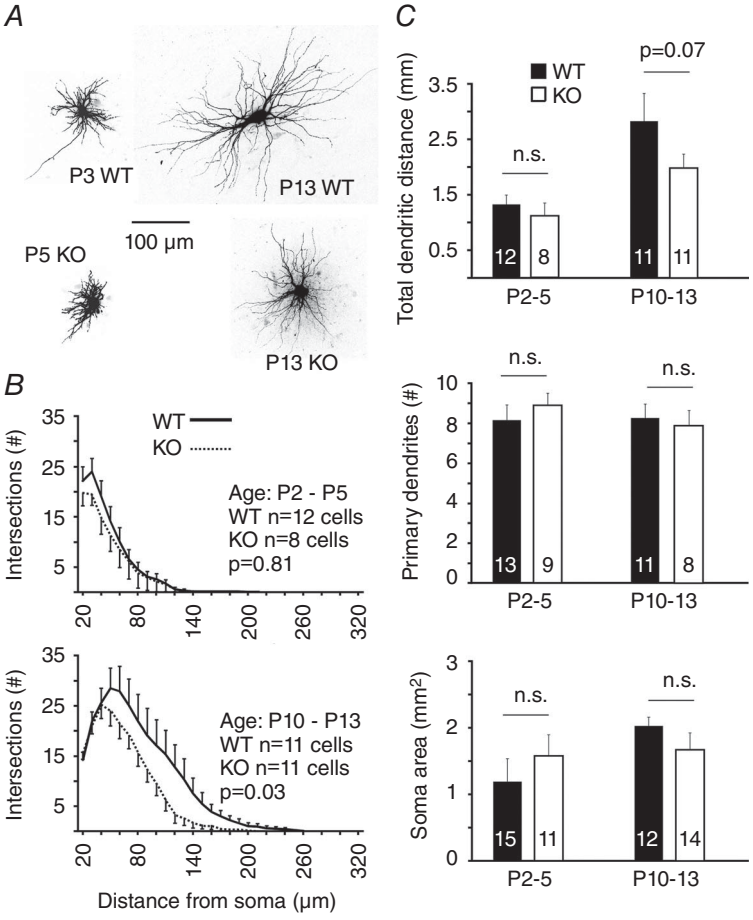

Figure 8. Morphology of VB neurons by Cx36 genotpye and age
A, photomicrographs of example neurons used for morphological analysis. *B*, counts of Sholl intersections by distance from the soma (mean ± SEM) by genotype and age group. *P* values are from a Kolmogorov–Smirnov test. *C*, morphological characteristics determined from Sholl intersections and 3-D reconstruction of somata. Numbers of sampled neurons for each group are indicated on the bars. n.s., not significant.

TRN cells in the Cx36 KO. Previous reports from our laboratory have also suggested that there is weak electrical coupling in Cx36 KO mice (Landisman *et al.* 2002), as well as some dye-coupling between Cx36 KO-TRN neurons (Lee *et al.* 2014). We conclude that TRN neurons can express functional gap junctions that lack Cx36, although we cannot say whether non-Cx36 junctions are present in WT cells or occur only as a compensatory response to Cx36 deletion. In principle, the relatively low-conductance gap junctions between KO neurons could arise from electrotonically distant connections that appear weak as a result of space clamp errors, or they may actually have reduced junctional conductance. The latter is more probable because Cx36 KO mice also have relatively small clusters of dye-coupled TRN neurons compared to WT neurons (Lee *et al.* 2014). It is not clear whether electrical coupling in the KO-TRN is relevant to network activity, as it is in the WT-TRN (Long *et al.* 2004). Non-Cx36 gap junctions might play a non-electrical role by allowing transfer of signalling molecules among neurons (Mese *et al.* 2007); consistent with this, dye-coupling is more evident than electrical coupling in the TRN of the Cx36 KO (Lee *et al.* 2014).

Surprisingly, we found that many electrical synapses in the KO-TRN had asymmetric G_j. Asymmetric G_j (i.e. rectification) is common among coupled neurons of invertebrates and some fish (Furshpan and Potter, 1959; Auerbach and Bennett, 1969; Rash *et al.* 2013), although reports of rectifying junctions in the mammalian brain are few and inconsistent (Devor and Yarom, 2002; Hoge *et al.* 2011). Interestingly, electrical coupling asymmetry was reported between rat TRN neurons under specific physiological conditions (Haas *et al.* 2011) and was shown to have a substantial influence on the spike timing relationship between coupled neurons (Sevetson and Haas, 2015). Because a few cases of WT electrical coupling were modestly asymmetrical (Fig. 3*B* and *C*), it is possible that some of the gap junctions present in the WT-TRN are non-Cx36-dependent.

Asymmetric G_j can occur in heterotypic gap junction channels, with each hemichannel comprised of different connexins (Barrio *et al.* 1992; He *et al.* 1999; Bukauskas *et al.* 2002). Heterotypic gap junctions underlie asymmetric G_j between coupled neurons of *Drosophila* (Phelan *et al.* 2008) and teleost fish (Rash *et al.* 2013). These results suggest that two or more connexins, neither of them Cx36, are expressed in some KO-TRN neurons. Two possibilities are Cx45 (Sohl *et al.* 2005) and Cx30.2 (Kreuzberg *et al.* 2008; Perez *et al.* 2010), which are both neuronal connexins expressed in the mouse thalamus. In expression systems, Cx45 and Cx30.2 can form heterotypic and heteromeric junctions with voltage-dependent decay kinetics intermediate between homotypic channels of either connexin alone (Kreuzberg *et al.* 2005; Gemel *et al.* 2008). These properties roughly fit the decay kinetics that we measured from electrical connections in TRN neurons of the Cx36 KO (Fig. 2*B*).

Cx36 and development of passive membrane properties

During postnatal development, neuronal R_{in} declined and C_{in} increased in both TRN and VB, consistent with previous studies (Warren and Jones, 1997; Parker *et al.* 2009; Lee *et al.* 2010). The mean R_{in} of TRN cells dropped six-fold between P2 and P13, possibly as a result of the addition of membrane leak channels and increased gap junctional conductance. The mean R_{in} of TRN neurons from KO mice was higher than that of WT cells. The presence of gap junctions tends to reduce R_{in} in other types of neurons (Deans *et al.* 2001; Amitai *et al.* 2002; Long *et al.* 2002). Similar differences of R_{in} between WT and Cx36 KO-TRN neurons were reported by Landisman *et al.* (2002) in P14–P18 mice. The electrical synapses among KO TRN neurons probably do not significantly contribute to input conductance. R_{in} of VB neurons was not influenced by Cx36 genotype, which is consistent with their weak electrical coupling postnatally (Lee *et al.* 2010).

The absence of most gap junctions among KO TRN neurons could have a direct effect on thalamic network function during development. A higher R_{in} amplifies voltage responses to synaptic inputs and lengthens the

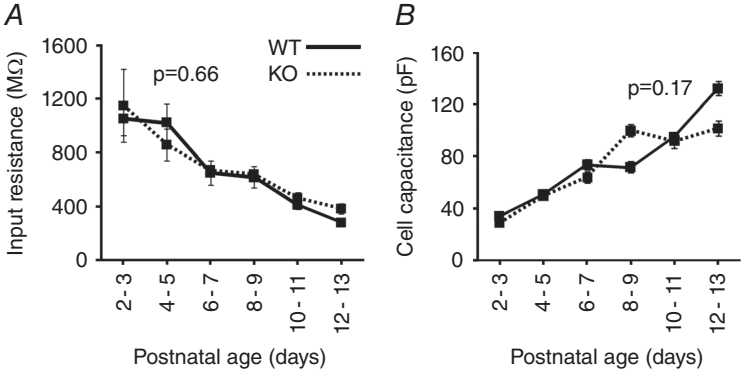

Figure 9. Passive membrane properties of VB neurons as a function of age and Cx36 genotype
A, input resistance declined with age but was unaffected by genotype ($P = 0.66$, $r = 0.73$). *B*, cell capacitance increased with age but was unaffected by genotype ($P = 0.17$, $r = 0.61$). *P* values were determined based on linear regression. A total of 138 neurons were sampled (71 WT and 67 KO neurons); *n* for each genotype per 2-day age group ranged from four to 15 neurons.

membrane time constant, which affects temporal and spatial integration and attenuates high-frequency events. This could be particularly important during development because network maturation depends strongly on the strength, and perhaps synchrony, of electrical activity (Catalano and Shatz, 1998; Dantzker and Callaway, 1998; Zhang and Poo, 2001).

Cx36 and development of inhibition and neuronal morphology

Synaptogenesis commences before birth in the mouse thalamus, and network formation continues for several weeks thereafter (Jones, 2007). We found significant increases in mIPSC frequency during the first postnatal week (Fig. 6*B*), which probably reflects rapid addition of GABA-releasing synapses. The mIPSC frequency levels out by P8, presumably as synaptogenesis ends; this is around the time when thalamic spindle oscillations begin to mature (Warren and Jones, 1997). Age also correlated strongly with mIPSC decay rate (Fig. 6*B*), probably as a result of the changing subunit composition of $GABA_A$ receptors (Laurie *et al.* 1992). The decay rate of IPSCs in VB is an important determinant of the frequency of spindle oscillations (Bal *et al.* 1995; Sohal *et al.* 2006). Deletion of Cx36 significantly increased mIPSC frequency in VB. This could be caused by more GABAergic synapses or increased spontaneous GABA release. It is also possible that increased dendritic length constants would allow distal IPSCs to propagate to somata more readily (Carnevale and Johnston, 1982). Because the evoked inhibitory paired-pulse ratio was not affected by genotype (Fig. 6*E*), and because the mIPSC frequency did not correlate with R_{in} (which may relate to dendro-somatic electrotonic coupling; data not shown), release probability or R_{in} probably do not account for this result (Prange and Murphy, 1999). We suggest that the deletion of Cx36 leads to an increased number of GABAergic release sites.

Both Cx36 and age affected the distribution of mIPSC amplitudes in VB neurons (Fig. 6*D*), which suggests alterations of synaptic vesicle size or neurotransmitter concentration, or the density of postsynaptic $GABA_A$ receptors. In general, there were fewer large mIPSCs in older cells. Overall, there is more inhibition in the thalamus of the Cx36 KO than in WT thalamus, probably resulting from homeostatic changes as a result of altered synaptic and network activity in the Cx36 KO.

We also found that Cx36 affected the development of neuron morphology. Most notably, VB dendritic fields were more complex in the WT compared to the KO, and TRN somata were larger in the P2–5 KO-TRN compared to the P2–5 WT-TRN. Interestingly, previous work on inferior olivary neurons showed that Cx36 KO alters dendritic thickness (De Zeeuw *et al.* 2003), perhaps implying a role for Cx36 in the maturation of neuron morphology.

The mechanisms driving these changes are unclear. Gap junctions may provide cell–cell adhesion (Elias *et al.* 2007), although the sparseness of coupling among developing VB neurons (Lee *et al.* 2010) argues against this. Gap junctions might pass morphologically important signalling molecules, although the non-Cx36 coupling among KO cells could provide such a role. Cell morphology can also be affected by neural activity (Parrish *et al.* 2007) and reduced electrical coupling could change firing rates or synchrony.

We found that Cx36 deletion leads to fewer VB neuron pairs with coincident IPSCs (Fig. 7*B*), which suggests fewer divergent inputs from TRN. Less complex dendritic trees in KO-VB neurons would reduce the ability of neighbouring neurons to capture inputs from a common presynaptic axon, and thus could lead to smaller receptive fields in VB. Less divergent input would also tend to reduce the influence of each TRN neuron on the VB neuron population, and therefore produce more specific feedforward and feedback inhibition in the thalamocortical network. Cx36 KO mice exhibit impaired function in cognitive and behavioural tasks (Allen *et al.* 2011; Zlomuzica *et al.* 2012), perhaps in part because of abnormal inhibitory synaptic properties. Taken together, our data strongly suggest that Cx36-dependent electrical coupling is necessary for the normal development of thalamic inhibitory networks.

Regulation of chemical synapse development by electrical synapses

Cx36 is important for regulating synchronized activity in central networks (Gibson *et al.* 1999; Landisman *et al.* 2002; Buhl *et al.* 2003; Long *et al.* 2004, 2005; Mancilla *et al.* 2007). Network synchronization during development may contribute to the stabilization of chemical synaptic connections by co-ordinating the activity of neighbouring synapses (Personius and Balice-Gordon, 2000). Desynchronization as a result of the loss of Cx36 might lead to more competition and pruning among synapses (Kim and Kandler, 2003). The TRN generates spontaneous activity during development, which has been implicated in chemical synaptic development in the thalamus (Pangratz-Fuehrer *et al.* 2007). Our findings suggest that the Cx36 KO has less divergent input from the TRN to VB neurons, perhaps because of desynchronized TRN activity and the consequent pruning of its inputs onto VB neurons. Gap junctions in the early postnatal TRN may contribute to patterns of spontaneous activity that support the subsequent maturation of chemical synapses in the thalamus.

References

Agmon A & Connors BW (1991). Thalamocortical responses of mouse somatosensory (barrel) cortex in vitro. *Neuroscience* **41**, 365–379.

Allen K, Fuchs EC, Jaschonek H, Bannerman DM & Monyer H (2011). Gap junctions between interneurons are required for normal spatial coding in the hippocampus and short-term spatial memory. *J Neurosci* **31**, 6542–6552.

Amitai Y, Gibson JR, Beierlein M, Patrick SL, Ho AM, Connors BW & Golomb D (2002). The spatial dimensions of electrically coupled networks of interneurons in the neocortex. *J Neurosci* **22**, 4142–4152.

Arumugam H, Liu X, Colombo PJ, Corriveau RA & Belousov AB (2005). NMDA receptors regulate developmental gap junction uncoupling via CREB signaling. *Nat Neurosci* **8**, 1720–1726.

Auerbach AA & Bennett MV (1969). A rectifying electrotonic synapse in the central nervous system of a vertebrate. *J Gen Physiol* **53**, 211–237.

Bal T, von Krosigk M & McCormick DA (1995). Synaptic and membrane mechanisms underlying synchronized oscillations in the ferret lateral geniculate nucleus in vitro. *J Physiol* **483 (Pt 3)**, 641–663.

Barrio LC, Suchyna T, Bargiello T, Xu LX, Roginski RS, Bennett MV & Nicholson BJ (1992). Gap junctions formed by connexins 26 and 32 alone and in combination are differently affected by applied voltage. *Proc Natl Acad Sci USA* **88**, 8410–8414.

Belluardo N, Mudo G, Trovato-Salinaro A, Le Gurun S, Charollais A, Serre-Beinier V, Amato G, Haefliger JA, Meda P & Condorelli DF (2000). Expression of connexin36 in the adult and developing rat brain. *Brain Res* **865**, 121–138.

Bennett MV (1966). Physiology of electrotonic junctions. *Ann NY Acad Sci* **137**, 509–539.

Bennett MV & Zukin RS (2004). Electrical coupling and neuronal synchronization in the mammalian brain. *Neuron* **41**, 495–511.

Blankenship AG, Hamby AM, Firl A, Vyas S, Maxeiner S, Willecke K & Feller MB (2011). The role of neuronal connexins 36 and 45 in shaping spontaneous firing patterns in the developing retina. *J Neurosci* **31**, 9998–10008.

Buhl DL, Harris KD, Hormuzdi SG, Monyer H & Buzsaki G (2003). Selective impairment of hippocampal gamma oscillations in connexin-36 knock-out mouse in vivo. *J Neurosci* **23**, 1013–1018.

Bukauskas FF, Angele AB, Verselis VK & Bennett MV (2002). Coupling asymmetry of heterotypic connexin 45/ connexin 43-EGFP gap junctions: properties of fast and slow gating mechanisms. *Proc Natl Acad Sci USA* **99**, 7113–7118.

Bukauskas FF, Kreuzberg MM, Rackauskas M, Bukauskiene A, Bennett MV, Verselis VK & Willecke K (2006). Properties of mouse connexin 30.2 and human connexin 31.9 hemichannels: implications for atrioventricular conduction in the heart. *Proc Natl Acad Sci USA* **103**, 9726–9731.

Carnevale NT & Johnston D (1982). Electrophysiological characterization of remote chemical synapses. *J Neurophysiol* **47**, 606–621.

Catalano SM & Shatz CJ (1998). Activity-dependent cortical target selection by thalamic axons. *Science* **281**, 559–562.

Connors BW, Benardo LS & Prince DA (1983). Coupling between neurons of the developing rat neocortex. *J Neurosci* **3**, 773–782.

Connors BW & Long MA (2004). Electrical synapses in the mammalian brain. *Annu Rev Neurosci* **27**, 393–418.

Dantzker JL & Callaway EM (1998). The development of local, layer-specific visual cortical axons in the absence of extrinsic influences and intrinsic activity. *J Neurosci* **18**, 4145–4154.

De Zeeuw CI, Chorev E, Devor A, Manor Y, Van Der Giessen RS, De Jeu MT, Hoogenraad CC, Bijman J, Ruigrok TJ, French P, Jaarsma D, Kistler WM, Meier C, Petrasch-Parwez E, Dermietzel R, Sohl G, Gueldenagel M, Willecke K & Yarom Y (2003). Deformation of network connectivity in the inferior olive of connexin 36-deficient mice is compensated by morphological and electrophysiological changes at the single neuron level. *J Neurosci* **23**, 4700–4711.

Deans MR, Gibson JR, Sellitto C, Connors BW & Paul DL (2001). Synchronous activity of inhibitory networks in neocortex requires electrical synapses containing connexin36. *Neuron* **31**, 477–485.

Devor A & Yarom Y (2002). Electrotonic coupling in the inferior olivary nucleus revealed by simultaneous double patch recordings. *J Neurophysiol* **87**, 3048–3058.

Elias LA, Wang DD & Kriegstein AR (2007). Gap junction adhesion is necessary for radial migration in the neocortex. *Nature* **448**, 901–907.

Fischbach GD (1972). Synapse formation between dissociated nerve and muscle cells in low density cell cultures. *Dev Biol* **28**, 407–429.

Froemke RC (2015). Plasticity of cortical excitatory–inhibitory balance. *Annu Rev Neurosci* **38**, 195–219.

Furshpan EJ & Potter DD (1959). Transmission at the giant motor synapses of the crayfish. *J Physiol* **145**, 289–325.

Gemel J, Lin X, Collins R, Veenstra RD & Beyer EC (2008). Cx30.2 can form heteromeric gap junction channels with other cardiac connexins. *Biochem Biophys Res Commun* **369**, 388–394.

Gibson JR, Beierlein M & Connors BW (1999). Two networks of electrically coupled inhibitory neurons in neocortex. *Nature* **402**, 75–79.

Harris AL (2001). Emerging issues of connexin channels: biophysics fills the gap. *Q Rev Biophys* **34**, 325–472.

Haas JS, Zavala B & Landisman CE (2011). Activity-dependent long-term depression of electrical synapses. *Science* **334**, 389–393.

He DS, Jiang JX, Taffet SM & Burt JM (1999). Formation of heteromeric gap junction channels by connexins 40 and 43 in vascular smooth muscle cells. *Proc Natl Acad Sci USA* **96**, 6495–6500.

Hensch TK & Fagiolini M (2005). Excitatory–inhibitory balance and critical period plasticity in developing visual cortex. *Prog Brain Res* **147**, 115–124.

Hoge GJ, Davidson KG, Yasumura T, Castillo PE, Rash JE & Pereda AE (2011). The extent and strength of electrical coupling between inferior olivary neurons is heterogeneous. *J Neurophysiol* **105**, 1089–1101.

Hormuzdi SG, Pais I, LeBeau FE, Towers SK, Rozov A, Buhl EH, Whittington MA & Monyer H (2001). Impaired electrical signaling disrupts gamma frequency oscillations in connexin 36-deficient mice. *Neuron* **31**, 487–495.

Huguenard JR & McCormick DA (2007). Thalamic synchrony and dynamic regulation of global forebrain oscillations. *Trends Neurosci* **30**, 350–356.

Huntsman MM & Huguenard JR (2000). Nucleus-specific differences in GABA(A)-receptor-mediated inhibition are enhanced during thalamic development. *J Neurophysiol* **83**, 350–358.

Jaslove SW & Brink PR (1986). The mechanism of rectification at the electrotonic motor giant synapse of the crayfish. *Nature* **323(6083)**, 63–65.

Jones EG (2007). *The Thalamus*, 2nd edn. Cambridge: Cambridge University Press.

Kandler K & Katz LC (1995). Neuronal coupling and uncoupling in the developing nervous system. *Curr Opin Neurobiol* **5**, 98–105.

Kandler K & Katz LC (1998*a*). Coordination of neuronal activity in developing visual cortex by gap junction-mediated biochemical communication. *J Neurosci* **18**, 1419–1427.

Kandler K & Katz LC (1998*b*). Relationship between dye coupling and spontaneous activity in developing ferret visual cortex. *Dev Neurosci* **20**, 59–64.

Kätzel D & Miesenböck G (2014). Experience-dependent rewiring of specific inhibitory connections in adult neocortex. *PLoS Biol* **12**, e1001798.

Kim G & Kandler K (2003). Elimination and strengthening of glycinergic/GABAergic connections during tonotopic map formation. *Nat Neurosci* **6**, 282–290.

Koval M, Molina SA & Burt JM (2014). Mix and match: investigating heteromeric and heterotypic gap junction channels in model systems and native tissues. *FEBS Lett* **588**, 1193–1204.

Kreuzberg MM, Sohl G, Kim JS, Verselis VK, Willecke K & Bukauskas FF (2005). Functional properties of mouse connexin30.2 expressed in the conduction system of the heart. *Circ Res* **96**, 1169–1177.

Kreuzberg MM, Deuchars J, Weiss E, Schober A, Sonntag S, Wellershaus K, Draguhn A & Willecke K (2008). Expression of connexin30.2 in interneurons of the central nervous system in the mouse. *Mol Cell Neurosci* **37**, 119–134.

Landisman CE, Long MA, Beierlein M, Deans MR, Paul DL & Connors BW (2002). Electrical synapses in the thalamic reticular nucleus. *J Neurosci* **22**, 1002–1009.

Laurie DJ, Wisden W & Seeburg PH (1992). The distribution of thirteen GABAA receptor subunit mRNAs in the rat brain. III. Embryonic and postnatal development. *J Neurosci* **12**, 4151–4172.

Lee SC, Cruikshank SJ & Connors BW (2010). Electrical and chemical synapses between relay neurons in developing thalamus. *J Physiol* **588**, 2403–2415.

Lee SC, Patrick SL, Richardson, KA & Connors BW (2014). Two functionally distinct networks of gap junction-coupled inhibitory neurons in the thalamic reticular nucleus. *J Neurosci* **34**, 13170–13182.

Lee SM, Friedberg MH & Ebner FF (1994). The role of GABA-mediated inhibition in the rat ventral posteriormedial thalamus. I. Assessment of receptive field changes following thalamic reticular nucleus lesions. *J Neurophysiol* **71**, 1702–1715.

Li Y, Lu H, Cheng PL, Ge S, Xu H, Shi SH & Dan Y (2012). Clonally related visual cortical neurons show similar stimulus feature selectivity. *Nature* **486**, 118–121.

Liu XB & Jones EG (2003). Fine structural localization of connexin-36 immunoreactivity in mouse cerebral cortex and thalamus. *J Comp Neurol* **466**, 457–467.

Long MA, Landisman CE & Connors BW (2004). Small clusters of electrically coupled neurons generate synchronous rhythms in the thalamic reticular nucleus. *J Neurosci* **24**, 341–349.

Long MA, Deans MR, Paul DL & Connors BW (2002). Rhythmicity without synchrony in the electrically uncoupled inferior olive. *J Neurosci* **22**, 10898–10905.

Long MA, Jutras MJ, Connors BW & Burwell RD (2005). Electrical synapses coordinate activity in the suprachiasmatic nucleus. *Nat Neurosci* **8**, 61–66.

Maher BJ, McGinley MJ & Westbrook GL (2009). Experience-dependent maturation of the glomerular microcircuit. *Proc Natl Acad Sci USA* **106**, 16865–16870.

Mancilla JG, Lewis TJ, Pinto DJ, Rinzel J & Connors BW (2007). Synchronization of electrically coupled pairs of inhibitory interneurons in neocortex. *J Neurosci* **27**, 2058–2073.

Mentis GZ, Diaz E, Moran LB & Navarrete R (2002). Increased incidence of gap junctional coupling between spinal motoneurones following transient blockade of NMDA receptors in neonatal rats. *J Physiol* **544**, 757–764.

Mese G, Richard G & White TW (2007). Gap junctions: basic structure and function. *J Invest Dermatol* **127**, 2516–2524.

Montoro RJ & Yuste R (2004). Gap junctions in developing neocortex: a review. *Brain Res Brain Res Rev* **47**, 216–226.

Moreno AP, Laing JG, Beyer EC & Spray DC (1995). Properties of gap junction channels formed of connexin 45 endogenously expressed in human hepatoma (SKHep1) cells. *Am J Physiol Cell Physiol* **268**, C356–C365.

Neunuebel JP & Zoran MJ (2005). Electrical synapse formation disrupts calcium-dependent exocytosis, but not vesicle mobilization. *Synapse* **56**, 154–165.

Niculescu D & Lohmann C (2013). Gap junctions in developing thalamic and neocortical neuronal networks. *Cereb Cortex* **24**, 3097–3106.

Pangratz-Fuehrer S, Rudolph U & Huguenard JR (2007). Giant spontaneous depolarizing potentials in the developing thalamic reticular nucleus. *J Neurophysiol* **97**, 2364–2372.

Parker PR, Cruikshank SJ & Connors BW (2009). Stability of electrical coupling despite massive developmental changes of intrinsic neuronal physiology. *J Neurosci* **29**, 9761–9770.

Parrish JZ, Emoto K, Kim MD & Jan YN (2007). Mechanisms that regulate establishment, maintenance, and remodeling of dendritic fields. *Annu Rev Neurosci* **30**, 399–423.

Pereda AE (2014). Electrical synapses and their functional interactions with chemical synapses. *Nat Rev Neurosci* **15**, 250–263.

Perez DESML, Dedek K, Janssen-Bienhold U, Meyer A, Kreuzberg MM, Lorenz S, Willecke K & Weiler R (2010). Expression and modulation of connexin30.2, a novel gap junction protein in the mouse retina. *Vis Neurosci* **27**, 91–101.

Personius KE & Balice-Gordon RJ (2000). Activity-dependent editing of neuromuscular synaptic connections. *Brain Res Bull* **53**, 513–522.

Personius KE, Chang Q, Mentis GZ, O'Donovan MJ & Balice-Gordon RJ (2007). Reduced gap junctional coupling leads to uncorrelated motor neuron firing and precocious neuromuscular synapse elimination. *Proc Natl Acad Sci USA* **104**, 11808–11813.

Phelan P, Goulding LA, Tam JL, Allen MJ, Dawber RJ, Davies JA & Bacon JP (2008). Molecular mechanism of rectification at identified electrical synapses in the *Drosophila* giant fiber system. *Curr Biol* **18**, 1955–1960.

Pinault D (2004). The thalamic reticular nucleus: structure, function and concept. *Brain Res Brain Res Rev* **46**, 1–31.

Prange O & Murphy TH (1999). Correlation of miniature synaptic activity and evoked release probability in cultures of cortical neurons. *J Neurosci* **19**, 6427–6438.

Rash JE, Curti S, Vanderpool KG, Kamasawa N, Nannapaneni S, Palacios-Prado N, Flores CE, Yasumura T, O'Brien J, Lynn BD, Bukauskas FF, Nagy JI & Pereda AE (2013). Molecular and functional asymmetry at a vertebrate electrical synapse. *Neuron* **79**, 957–969.

Roerig B & Feller MB (2000). Neurotransmitters and gap junctions in developing neural circuits. *Brain Res Brain Res Rev* **32**, 86–114.

Sevetson J & Haas JS (2015). Asymmetry and modulation of spike timing in electrically coupled neurons. *J Neurophysiol* **113**, 1743–1751.

Sholl DA (1953). Dendritic organization in the neurons of the visual and motor cortices of the cat. *J Anat* **87**, 387–406.

Sohal VS, Pangratz-Fuehrer S, Rudolph U & Huguenard JR (2006). Intrinsic and synaptic dynamics interact to generate emergent patterns of rhythmic bursting in thalamocortical neurons. *J Neurosci* **26**, 4247–4255.

Sohl G, Maxeiner S & Willecke K (2005). Expression and functions of neuronal gap junctions. *Nat Rev Neurosci* **6**, 191–200.

Sutor B & Hagerty T (2005). Involvement of gap junctions in the development of the neocortex. *Biochim Biophys Acta* **1719**, 59–68.

Szabo TM & Zoran MJ (2007). Transient electrical coupling regulates formation of neuronal networks. *Brain Res* **1129**, 63–71.

Szabo TM, Faber DS & Zoran MJ (2004). Transient electrical coupling delays the onset of chemical neurotransmission at developing synapses. *J Neurosci* **24**, 112–120.

Teubner B, Degen J, Sohl G, Guldenagel M, Bukauskas FF, Trexler EB, Verselis VK, De Zeeuw CI, Lee CG, Kozak CA, Petrasch-Parwez E, Dermietzel R & Willecke K (2000). Functional expression of the murine connexin 36 gene coding for a neuron-specific gap junctional protein. *J Membr Biol* **176**, 249–262.

Todd KL, Kristan WB, Jr. & French KA (2010). Gap junction expression is required for normal chemical synapse formation. *J Neurosci* **30**, 15277–15285.

Van Rijen HV, Wilders R, Van Ginneken AC & Jongsma HJ (1998). Quantitative analysis of dual whole-cell voltage-clamp determination of gap junctional conductance. *Pflügers Arch* **436**, 141–151.

Warren RA & Jones EG (1997). Maturation of neuronal form and function in a mouse thalamo-cortical circuit. *J Neurosci* **17**, 277–295.

Willecke K, Eiberger J, Degen J, Eckardt D, Romualdi A, Guldenagel M, Deutsch U & Sohl G (2002). Structural and functional diversity of connexin genes in the mouse and human genome. *Biol Chem* **383**, 725–737.

Yu YC, He S, Chen S, Fu Y, Brown KN, Yao XH, Ma J, Gao KP, Sosinsky GE, Huang K & Shi SH (2012). Preferential electrical coupling regulates neocortical lineage-dependent microcircuit assembly. *Nature* **486**, 113–117.

Zhang LI & Poo MM (2001). Electrical activity and development of neural circuits. *Nat Neurosci* **4** (Suppl), 1207–1214.

Zlomuzica A, Viggiano D, Degen J, Binder S, Ruocco LA, Sadile AG, Willecke K, Huston JP & Dere E (2012). Behavioral alterations and changes in Ca/calmodulin kinase II levels in the striatum of connexin36 deficient mice. *Behav Brain Res* **226**, 293–300.

Additional information

Competing interests

The authors declare that they have no competing interests.

Author contributions

TAZ and BWC conceived and designed the experiments. TAZ and BWC collected, assembled, analysed and interpreted the data. All experiments were performed in the laboratory of BWC at Brown University. TAZ and BWC drafted the article or revised it critically for important intellectual content. Both authors have approved the final version of the manuscript and agree to be accountable for all aspects of the work. All persons designated as authors qualify for authorship, and all those who qualify for authorship are listed.

Funding

This research was supported by grants from the NIH: NRSA grant NS060448 (to TAZ), NS050434 (to BWC); and from the NSF: EFRI-0937848 (to BWC).

Acknowledgements

We thank Saundy Patrick for excellent technical assistance and Omar Ahmed for helping with the Matlab code.